Journal of Sound and Vibration (2003) **259**(1), 1–16
doi:10.1006/jsvi.2002.5076, available online at http://www.idealibrary.com on IDEAL®

THE APPLICATION OF PSEUDO-PHASE PORTRAIT IN MACHINE CONDITION MONITORING

W. J. Wang and R. M. Lin

Centre for Mechanics of Micro-Systems, School of Mechanical & Production Engineering, Nanyang Technological University, Singapore 639798*, Singapore. E-mail: mwjwang@ntu.edu.sg*

(*Received* 29 *August* 2001*, and in final form* 21 *February* 2002)

This paper presents a robust phase space reconstruction method based on singular value decomposition technique and its applications to large rotating machine and gear system condition monitoring and fault diagnosis. The singular value decomposition is used to determine the effective embedding space and to reduce the noise level of a measured vibration signal. Following the singular value decomposition, a pseudo-phase portrait can be obtained in the effective embedding space. This pseudo-phase portrait is then used to extract qualitative features of machine faults. Experience has shown that when one compares the pseudo-phase portraits obtained under different machine conditions, it is often possible to detect major differences due to different dynamic and kinematic mechanisms. In the case of gear system condition monitoring, correlation dimension has been introduced to evaluate these differences in order to obtain more accurate and reliable diagnosis. The pseudo-phase portrait is conceptually simple and has been found to be sensitive to some fault types. It is promising therefore that such pseudo-phase portraits can be used to realize real-time, online computer-aided diagnosis of machine faults.

1. INTRODUCTION

It is well known that failure of a mechanical system is always accompanied with the changes of its dynamic characteristics, usually from a linear or weak non-linear behavior to a strongly non-linear vibration response. In a rotating machine in which faults exist, one generally observes complicated non-linear vibration characteristics. Chaotic motions can be found in a large rotating machine with an unstable oil film, a cracked rotor, a rotor-to-stator rub or a loose pedestal [1–5]. Various non-linear dynamics including chaotic vibrations can be found in gear systems [6]. Therefore, for effective fault diagnosis, it is necessary to develop non-linear diagnostic methods in addition to those methods currently in use, such as orbit portrait, FFT spectrum, cepstrum and time–frequency or time-scale analysis, etc.

In recent years, the advancement of the theoretical development of non-linear dynamics has brought about new methodologies which can be employed to identify and forecast complex non-linear vibration behavior. Diagnostic modules based on both qualitative (e.g., the Poincaré map, the bifurcation diagram and the pseudo-phase portrait, etc.) and quantitative (e.g., the Lyapunov exponents, the correlation dimension and the Kolmogorov entropy, etc.) chaos indicators have made it possible for the early detection of the presence of chaotic operating conditions. Adams and Abu-Mahfouz [7] examined rotor rub impact and reported their comparison studies between the results obtained with conventional FFT and orbit techniques and those with the Poincaré map. These studies

0022-460X/02/$35.00

have shown that one can detect changes in both the pattern of the Poincaré map and the fractal dimension while neither the FFT nor the vibration orbit can show these changes clearly. The application of the pseudo-phase portrait to large rotating machine fault diagnosis has been reported in our previous paper [8], where results have demonstrated that the pseudo-phase portrait seems to be simple for computer implementation and is sensitive to some fault types in large rotating machines. The correlation dimension has also been widely used as a powerful tool for interpreting irregular signals for engineering applications. Researchers have explored the potential applications of correlation dimension in machine condition monitoring and fault diagnosis [9–12].

Non-linear dynamic systems have been found to be most easily understood when viewed from a phase space perspective. If all variables are measurable, the phase portrait and the dynamic invariants can be obtained directly from the actual phase space formed by these variables. However, for a general multi-dimensional dynamic system, most measurement facilities or condition monitoring modules will only be able to obtain few of the variables which contribute to the dynamics of the system and the actual phase space of the system can rarely be obtained in practice. Moreover, for a real vibration signal, one can neither derive nor build the phase portrait analytically due to the unavailability of the differential equations of the system. In order to overcome these problems, Takens introduced the embedding theorem [13]. Some of the important results are as follows: (1) it is possible to build an attractor simply by replacing the derivatives with delayed repetitions of only one measured variable of the system; (2) in order to evaluate the main characteristics of a process it is sufficient to build one attractor using only one of the variables measured as mentioned because each of these variables is strictly connected and contributes to each other.

Some important issues regarding the practical application of the embedding theorem should be considered carefully. Several remarks on this are given below.

Firstly, reconstruction parameters, such as lag time and embedding dimension, must be determined before reconstructing the state space. Takens' theorem assumes the availability of an infinite amount of measured noise-free data and imposes no restrictions on the selection of lag time τ, while for the embedding dimension m, it establishes the sufficient condition as $m \geqslant 2D + 1$, where D is the fractal dimension. However, since real measured data sets are finite and contaminated by noise, the embedding dimension and lag time must be correctly chosen so that the original system and its reconstructed counterpart are qualitatively equivalent. Only when this is ensured, further calculation carried out in this pseudo-phase space would give reliable results.

Secondly, experimentally derived signals are always affected by measurement noise. The pseudo-phase portrait and the dynamic invariants have been found to be sensitive to the presence of noise. For non-linear dynamics analysis, noise reduction techniques should be employed to eliminate noise components in a vibration signal while its chaotic components should be kept unmodified.

Finally, the phase space reconstructed from a vibration signal is multi-dimensional. The pseudo-phase portrait is in fact a projection of the multi-dimensional attractor in the pseudo-phase space. Major features of the attractor, including the number of fixed points, stability properties, and the disposition of the flow should be preserved to the fullest extent in the projected and normally two-dimensional pseudo-phase portrait. To achieve these requirements, the plane of projection of the attractor must be selected carefully.

This paper presents a robust phase space reconstruction method based on singular value decomposition technique and its applications to large rotating machine and gear system condition monitoring and fault diagnosis. The structure of this paper is as follows: in section 2, the basic non-linear dynamics analysis procedure is introduced. Section 3

researches the application of phase space reconstruction to real data measured from large rotating machines and gear systems. Extensive analysis results are given to verify the proposed method. Finally, conclusions are made in section 4.

2. PHASE SPACE RECONSTRUCTION

The main idea of the embedding theorem is that it is unnecessary to know the derivatives to form a co-ordinate system in which one can capture the structure of orbits. One can instead use directly the lagged variables to construct the state space.

For an N-point time series, $\{x_1, x_2, \ldots, x_N\}$, a sequence of vectors y_i in a new space can be generated as

$$y_i = \{x_i, x_{i+\tau}, \ldots, x_{i+(m-1)\tau}\}, \qquad \text{where } i = 1, 2, \ldots, N_m, \tag{1}$$

where $N_m = N - (m-1)\tau$ is the length of the reconstructed vectors y_i, m is the embedding dimension of the reconstructed state space, τ is called the lag time measured in units of sampling interval. The m co-ordinates of each point y_i are samples from the raw time series (separated by a fixed τ) covering an embedding window of length $\tau_w = (m-1)\tau$. The space which is reconstructed from a raw time series will be called the embedding space or pseudo-phase space and its dimension the embedding dimension. The trajectory in the pseudo-phase space is called the pseudo-phase portrait.

The reconstruction process consists of the determinations of the optimal lag time and the embedding dimension. In the literature of non-linear dynamics, several methods have been developed to determine these key parameters. The use of different time lags for each test can lead to large errors due to inaccurate and inappropriate choice of the lag time. On the other hand, the use of a constant lag time is also incorrect since each test has its own specific lag time. The lag time can be determined by autocorrelation function [14], mutual information [15], fill factor [16], wavering product [17], and high order correlation [18], etc. The attractor has been found to have more regular appearance when embedded in a space with adequate dimension than that with insufficient dimension. The approach taken in published work has been to increase m systematically, until trajectories no longer appear to intersect [19]. This is, at best, a rather subjective criterion, and the method is rapidly becoming inapplicable as the dimensions become higher or the noise is present. Another method, which seems to offer a better solution to this problem, is based on the algorithm of expansion of the process to the well-adapted basis, which was created by Neymark for optimal coding of biomedical information [20]. The potential applications of this algorithm to dynamical system phase space transformation and determination of embedding dimension were studied in reference [21].

In this paper, we introduce a more versatile singular value decomposition technique for the determination of the embedding dimension. The idea behind this approach is, given the hyperspace of dimension L, to find the smallest subspace that approximately bounds the attractor. This subspace is spanned by the eigenvectors corresponding to the largest eigenvalues of the covariance matrix of a time series, i.e., the directions where the attractor has the largest variance [22].

For a given time series, the singular spectrum may depend only on the choice of the embedding window length, not separately on the embedding dimension m, or the lag time τ [8, 22–24]. Therefore, the embedding window length τ_w, as an independent parameter instead of focusing on the parameters τ and m should be firstly determined. Kugiumtzis [23] suggested to set $\tau_w > \tau_p$, where τ_p is the mean orbital period which is equal to the mean *time between peaks* (tbp) of the raw time series. Here, we introduce another method to

determine τ_w. τ_w is defined as the average time that is needed to complete a full cycle after the first passage through the average of the signal [25].

For a given τ_w, one may select a sufficiently large L, and then construct trajectory matrix, A as

$$A = N_L^{-1/2}[y_1^{\mathrm{T}}, y_2^{\mathrm{T}}, \ldots, y_{N_L}^{\mathrm{T}}]^{\mathrm{T}}, \tag{2}$$

where $N_L^{-1/2}$ is a normalization coefficient. Then the covariance matrix B can be expressed as

$$B = A^{\mathrm{T}}A = \frac{1}{N_L}\sum_{i=1}^{N_L} y_i y_i^{\mathrm{T}}$$

$$= \frac{1}{N_L}\begin{bmatrix} \sum_{i=1}^{N_L} x_i x_i & \cdots & \sum_{i=1}^{N_L} x_i x_{i+(j-1)\tau} & \cdots & \sum_{i=1}^{N_L} x_i x_{i+(l-1)\tau} \\ \vdots & \vdots & \vdots & \vdots & \vdots \\ \sum_{i=1}^{N_L} x_{i+(j-1)\tau} x_i & \cdots & \sum_{i=1}^{N_L} x_{i+(j-1)\tau} x_{i+(j-1)\tau} & \cdots & \sum_{i=1}^{N_L} x_{i+(j-1)\tau} x_{i+(l-1)\tau} \\ \vdots & \vdots & \vdots & \vdots & \vdots \\ \sum_{i=1}^{N_L} x_{i+(l-1)\tau} x_i & \cdots & \sum_{i=1}^{N_L} x_{i+(l-1)\tau} x_{i+(j-1)\tau} & \cdots & \sum_{i=1}^{N_L} x_{i+(l-1)\tau} x_{i+(l-1)\tau} \end{bmatrix}, \tag{3}$$

where B is a real, symmetric $L \times L$ matrix, and hence its eigenvectors form a complete orthonormal basis in R^L. Assume that the eigenvalues of the covariance matrix B are ordered in a descending order as $\lambda_1 \geqslant \lambda_2 \geqslant \cdots \geqslant \lambda_L$. Then the normalized singular spectrum $\sigma_j \sim L(\sigma_j = |\lambda_j| / \sum_{j=1}^{L} |\lambda_j|$ are plotted.

In order to demonstrate the relationship between the normalized singular value and the choice of the embedding window length, the normalized singular spectrum of the Lorenz model is computed for different lag times but for the same window length. The Lorenz model is defined by the following equations [26]:

$$\dot{x} = a(y - x), \quad \dot{y} = px - y - xz, \quad \dot{z} = xy - bz, \tag{4}$$

where $a = 10$, $p = 28$, $b = 8/3$. In this instance, the system produces turbulent dynamics. The differential equations are solved numerically using a fourth order Runge–Kutta integration with a desired accuracy of 10^{-6}.

Figure 1(a) shows the normalized singular spectrum of the x variable of the Lorenz model versus the index for different values of τ in the case when $m = 6$. From Figure 1(a), one can see that the normalized singular spectra depend on τ significantly. Figure 1(b) shows the normalized singular spectra versus the index for a number of embedding

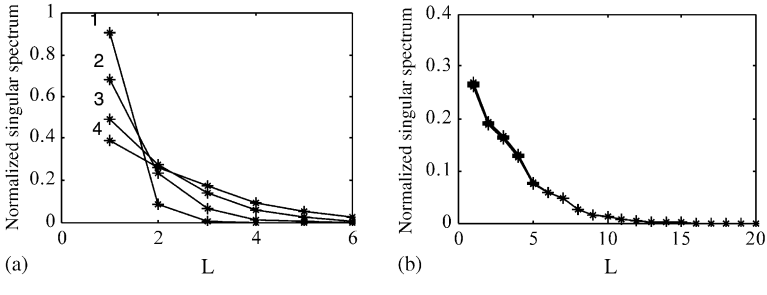

Figure 1. The normalized singular spectrum of data generated by the Lorenz equations: (a) The normalized singular spectrum plotted as a function of τ while for $m = 6$, curves 1, 2, 3 and 4 correspond to $\tau = 1, 4, 8$ and 12. (b) The values of embedding dimension and lag time are $(m, \tau) = (11,12)$, (13,10), (16,8), (21,6).

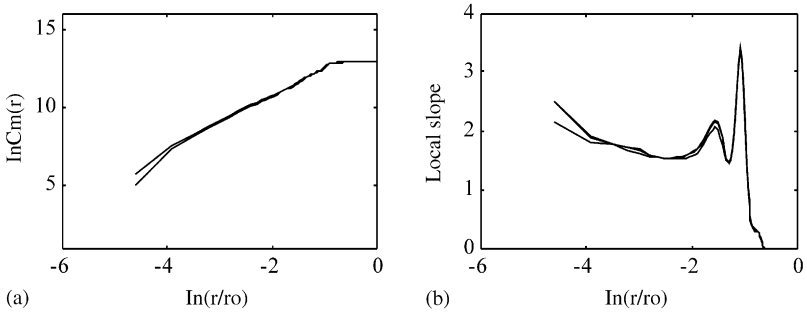

Figure 2. The estimation of correlation dimension for data generated by the Lorenz model. The values of embedding dimension and lag time are $(m, \tau) = (11,12)$, (13,10), (16,8), (21,6).

window lengths that are equal. The values of the embedding dimension and the lag (m, τ) used in the simulation were (11,12), (13,10), (16,8), and (21,6). They are seen to fall essentially on a singular curve. Figure 1(b) demonstrates the dependence of normalized singular spectrum on window length rather than separately on the embedding dimension and the lag time.

The embedding window length is of particular importance since it determines the amount of information passed from the time series to the embedding vectors. In order to study the effects of the embedding window length on the quality of the reconstruction, the correlation dimension of the x variable of the Lorenz model, which is used to assess the quality of the reconstruction, is computed for different lag times but for the same window length. Figure 2 shows the relative effects on the correlation dimension by varying both the lag time and the embedding dimension while keeping the window length constant. From Figure 2, one can see that all these cases follow a universal law.

The most valuable property of the normalized singular spectrum is that the embedding dimension can be determined in the absence of any prior knowledge about the dynamic system. Furthermore, the singular spectrum has the ability to discriminate the genuine signal components and those of the contaminated noise in the time series. In the absence of prior knowledge about the embedding dimension and the contamination, it is plausible to assume that the system state space is rather high dimensionally and that the noise will fill in low-dimensional state space more or less uniformly. The rank of the covariance matrix, which is equal to the number of its non-zero eigenvalues, is the dimension of the smallest subspace of the embedding space that contains the reconstructed trajectory. Let the observations be composed of signal $x(n)$ and noise $c(n)$: $y(n) = x(n) + c(n)$, where noise $c(n)$ prevents any eigenvalue of the covariance matrix from vanishing. The first major singular values, which are significantly large and represent the main components of the total signal energy, are selected to construct the "clean" signal. The corresponding subspace is regarded as the effective embedding space and its dimension the embedding dimension. The remaining singular values, which should otherwise be zero, are completely due to the presence of noise. In this case, it is possible to find a "noise floor" that arises from noise by investigating the singular values of the covariance matrix. Therefore, by imposing that those extra singular values due to noise be zero, a great amount of noise can be eliminated.

Once the embedding dimension is determined, the lag time can then be calculated according to the known relationship among the embedding window length, the lag time and the embedding dimension. According to the new embedding dimension and lag time,

the new covariance matrix will again be constructed. Then one can consider the two eigenvectors $\{C_1\}$ and $\{C_2\}$ which are associated with the maximum eigenvalues of the new covariance matrix as the two principal axes, and project the reconstructed attractor onto this plane spanned by $\{C_1\}$ and $\{C_2\}$. One can conclude that the reconstructed pseudo-phase portrait based on these procedures will possess all the major features of the dynamic characteristics of the system under consideration. Firstly, one may think of the trajectory as exploring on average, an m-dimensional ellipsoid. The $\{C_i\}$ then determine the directions and λ_i the lengths of the principal axes of the ellipsoid. Secondly, in the directions associated with larger eigenvalues, the effect of noise will be reduced, and in the directions associated with smaller or vanishing eigenvalues, the contribution of noise will dominate.

3. APPLICATIONS TO REAL VIBRATION SIGNALS

While numerically simulated signals may be useful for the preliminary research, experimental or industrial data are usually required for the evaluation and validation of a diagnostic system. In this section, the application of the proposed pseudo-phase portrait to gear damage detection and large rotating machine fault diagnosis will be evaluated from the point of view of the practitioners.

3.1. LARGE ROTATING MACHINE WITH FAULTS

In practice, a large rotating machine may experience various faults such as misalignment, imbalance, rotor-to-stator rub, surge, crack, oil whirl, oil whip, loose pedestal, and aerodynamic excitation, etc. Current condition monitoring systems for large rotating machine rely heavily upon signal processing techniques which were developed to deal with linear systems and were dominated by FFT-based analysis. Unfortunately, the application of linear spectral methods to data measured from non-linear systems can result in featureless spectrum which obscure the potential simplicity of the underlying non-linear mechanism. For example, a peak frequency of $0.4f - 0.5f$ (where f is the fundamental frequency) may correspond to either oil whirl or aerodynamic excitation or some other fault.

Figure 3 shows the FFT spectra of the vibration signals in a large rotating machine with an oil whirl fault and aerodynamic excitation fault. The spectra of these two conditions are so similar that one may fail to make a correct diagnostic decision based on spectral

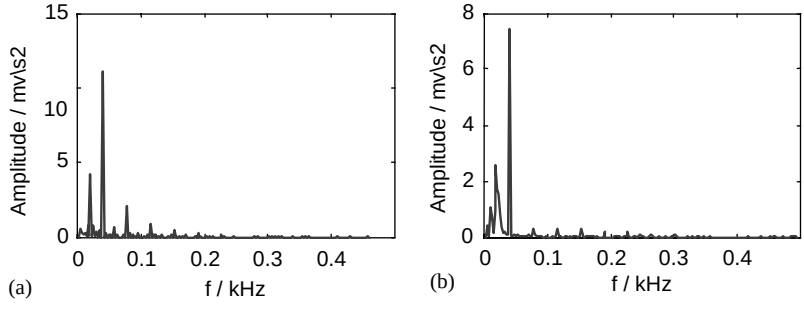

Figure 3. FFT spectra of the vibration signals of a large rotating machine with (a) oil whirl fault and (b) aerodynamic excitation fault.

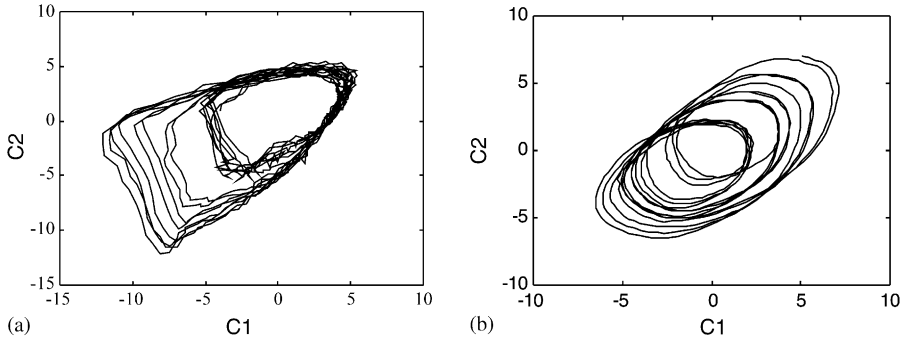

Figure 4. Pseudo-phase portraits reconstructed from the vibration signals of a large rotating machine with (a) oil whirl and (b) aerodynamic excitation. The ($C1$, $C2$) plane is spanned by two eigenvectors associated with the two largest eigenvalues of the covariance matrix.

analysis alone in this situation. However, the pseudo-phase portrait of the vibration signals in a large rotating machine with aerodynamic excitation fault is different from that of oil whirl fault. This can be seen clearly in Figure 4. Figure 4(a) shows the pseudo-phase portrait reconstructed from vibration signal of a large rotating machine with an unstable oil film. From Figure 4(a), one can see that the whirl phenomenon has been detected by pseudo-phase portrait. Figure 4(b) shows the pseudo-phase portrait of a large rotating machine with aerodynamic excitation fault. The location of the center of the pseudo-phase portrait is complicated and it changes along the 45^{o} direction.

The great influence of the lag time on the pseudo-phase portrait can be seen from Figure 5, which shows that the pseudo-phase portraits with different lag times. It can be seen that the change of lag time affects significantly the shape of the pseudo-phase portrait and it loses its coherent structure when the lag time increases above a characteristic value (optimal lag time). If τ is too small, the reconstructed attractor falls on the main diagonal of the co-ordinate system. This results in little information gain, i.e., redundance. If τ is too large, successive delay co-ordinates may become causally unrelated, leading to another extremity where the reconstruction is no longer representative of the true dynamics, and this is called irrelevance.

Figure 6(a) shows the pseudo-phase portrait reconstructed from the vibration signal of a large rotating machine with a slight rotor-to-stator rub fault. From Figure 6(a), one can see that there exist discontinuous points or sharp corners in the pseudo-phase portrait when a rotor-to-stator rub fault happens in a large rotating machine. Therefore, even if a slight rub fault happens in a large rotating machine, the pseudo-phase portrait can be used to diagnose it effectively. A very interesting phenomenon can be seen from Figure 6(b), which demonstrates the pseudo-phase portrait of the vibration signal of a large rotating machine with a serious rotor-to-stator rub fault. In comparison with Figure 6(a), there exist more sharp corners and direction changes. In essence, with the help of the pseudo-phase portraits shown in Figure 6, one can easily detect how a rotor-to-stator rub occurs and develops.

Figure 7(a) and 7(b) shows the pseudo-phase portraits reconstructed from the vibration signals of a large rotating machine with oil whip fault and loose pedestal fault respectively. From Figure 7(a), one can see that the changes of the position of the center of the pseudo-phase portrait are very complicated. This implies that the rotor system is severely unstable. When the loose pedestal condition and rotor-to-stator rub happen in a large rotating machine, they produce the same physical phenomena: impacting and periodic changes of

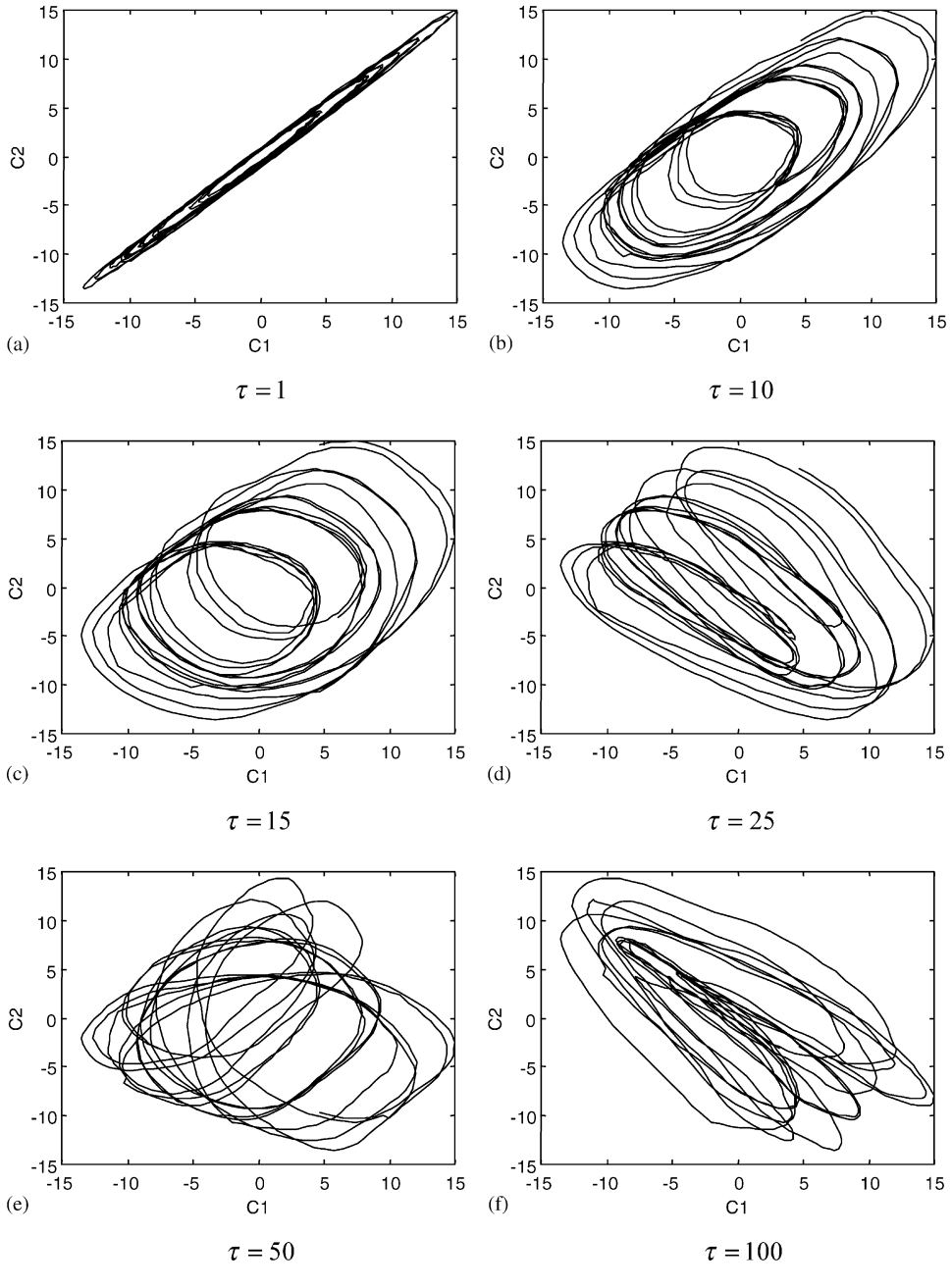

Figure 5. Pseudo-phase portraits reconstructed from the vibration signals of a large rotating machine with different lag times.

stiffness. It is hence rather difficult to classify these two faults using traditional diagnosis methods such as FFT spectra analysis. Fortunately however, the pseudo-phase portrait of the loose pedestal fault (as shown in Figure 7(b)) in a large rotating machine is different from that of rotor-to-stator rub (Figure 6). The friction due to rotor-to-stator rubbing plays an additionally important role which can be reflected by the discontinuous points or sharp corners in the pseudo-phase portrait as shown in Figure 6.

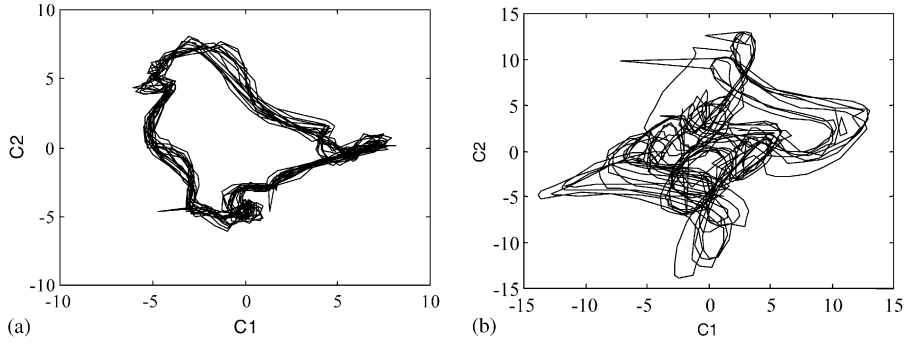

Figure 6. Pseudo-phase portraits reconstructed from the vibration signals of a large rotating machine with (a) slight rotor-to-stator rub fault and (b) serious rotor-to-stator rub fault.

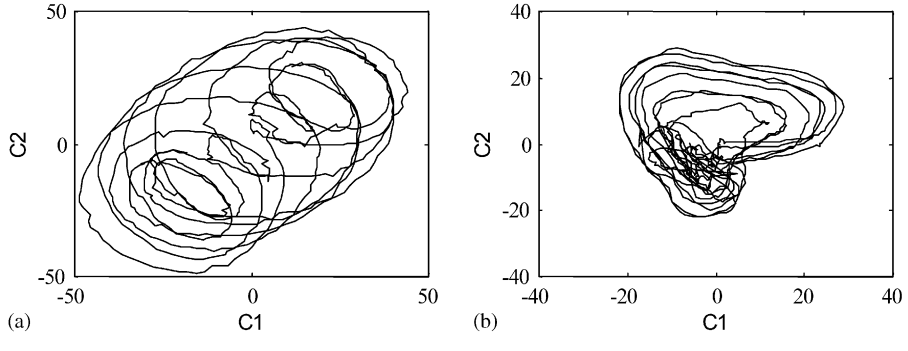

Figure 7. Pseudo-phase portraits reconstructed from the vibration signals of a large rotating machine with (a) oil whip fault and (b) loose pedestal fault.

From the above analysis, one can see that the pseudo-phase portraits are sensitive to some fault types in a large rotating machine. The change of the shape and position of the pseudo-phase portrait are important indications which can be employed to diagnose effectively fault sources and types. In general, when one compares the pseudo-phase portraits related to different conditions of a large rotating machine, it is often possible to find some differences due to different dynamic and kinematic mechanisms. Therefore, it is promising that the proposed pseudo-phase portrait method can be used to realize the real-time, online computer-aided diagnosis of large rotating machines.

3.2. GEAR SYSTEM FAULT DETECTION

A gear transmission system converts a rotary input motion into another rotary output motion at a different frequency. In an ideal mechanism, the relationship between input and output depends only on the geometry or kinematics of the meshing gears. However, for real industrial gear systems, many non-linear effects prevent them from being ideal, such as gaps and friction, leading to a very complex dynamic behavior of the meshing mechanism. Classical Fourier-transform-based analysis is generally difficult to use to detect gear system failures at an early stage. For this reason, researchers have proposed

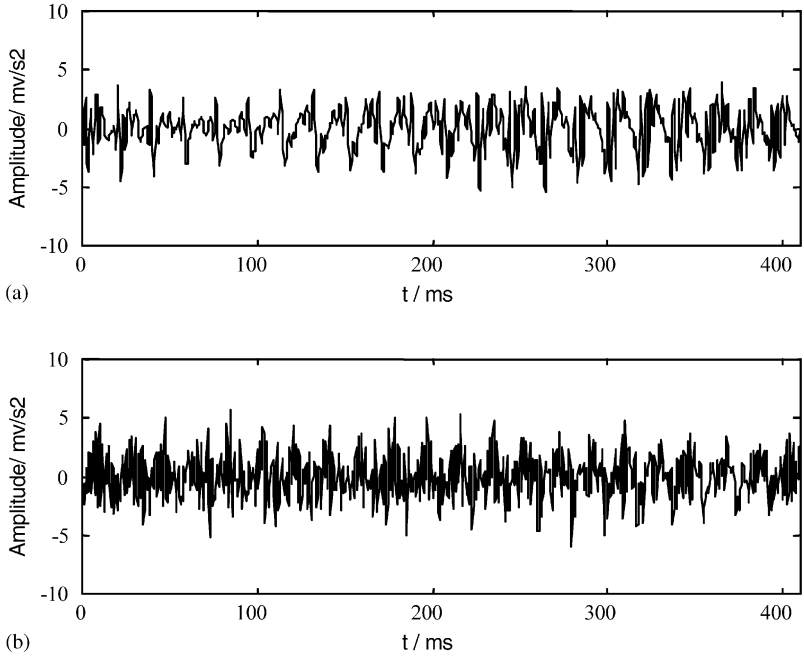

Figure 8. Gear system vibration signals of different operating conditions: (a) normal and (b) with early fatigue cracked tooth.

many other vibration analysis techniques for the early detection of gear systems fault symptoms, including the cepstra approach [27], the amplitude and phase demodulation approach [28], the cyclostationary process theory [29], and the time–frequency analysis [30, 31]. However, understanding of non-linear dynamics in gear systems has been very limited and largely neglected. Modern developments in non-linear dynamics have provided new tools to deal with this hitherto unsolved problem.

Figure 8 shows the vibration signals in a gear system under different operating conditions: normal and early fatigue crack. The experimental vibration signals were obtained from a system comprising an input gear with 23 teeth driven by an electric motor, and meshing with a driven gear of 22 teeth. The rotational frequency of the electric motor was 24 Hz which resulted in a meshing frequency of 552 Hz. The vibration signals were measured in the horizontal direction at the bearing housing and the sampling frequency was chosen as 2·5 kHz.

Figure 9 shows the pseudo-phase portraits resconstructed from the vibration signals shown in Figure 8. It can be seen from Figure 9 that the pseudo-phase portrait of the gear system under normal condition is more broad and regular than that obtained under cracked tooth condition.

Another experimental set-up contains a two-stage reduction gearbox. In the gear fatigue testing experiment, two pairs of gear (26-43, 36-24) came into meshing with the input rotating speed at 1270 r.p.m. During the gear fatigue testing process, the gearbox operating condition experienced three different stages: normal, with a cracked tooth and with a broken tooth. The gearbox translational vibration signals were measured externally on the gearbox-bearing case using an acceleration sensor and amplified by a charge amplifier to monitor the operating condition of the gearbox. The sampling frequency was chosen as 2·5 kHz.

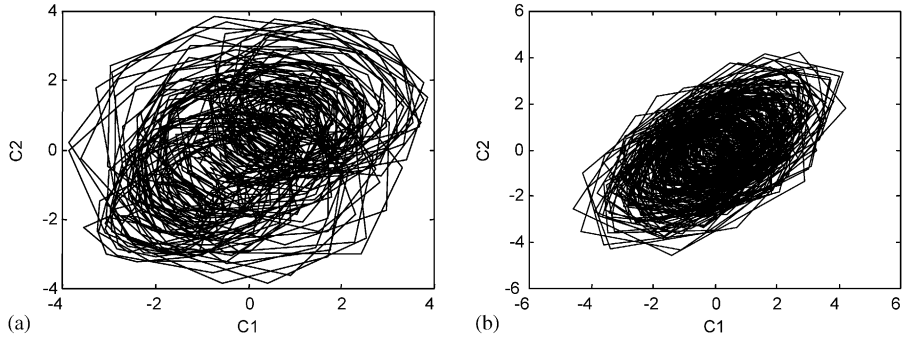

Figure 9. Pseudo-phase portraits of gear system vibration signals corresponding to different running conditions: (a) normal and (b) with early fatigue cracked tooth.

Raw vibration signals measured from the outside of the gearbox under different operating conditions are displayed as shown in Figure 10. Obviously, there are distinct differences between the vibration signals of the gearbox with a broken tooth and those of the other two operating conditions, but there is only a slight difference between the vibration signals measured under normal condition and the condition with a cracked tooth. As is well known, it is also very difficult to detect the existence of an early fatigue crack against normal operating condition by just using FFT and other frequency domain analysis. The pseudo-phase portraits of the vibration signals are illustrated in Figure 11. As shown in Figure 11, it becomes possible to identify the existence of cracked tooth against the normal operating condition from the pseudo-phase portraits.

From the above analysis, one can see that the pseudo-phase portrait has great potential for the reliable diagnosis of defects in industrial gear systems. However, unlike the pseudo-phase portraits of large rotating machine with faults, the pseudo-phase portraits appear as a very complicated solid with an undefined shape for the industrial gear systems. Although one usually compares the pseudo-phase portraits under different conditions of a gear system, it is also possible to establish some differences due to their different dynamic and kinematic mechanisms. More accurate characterization of these differences may be needed for effectively detecting gear systems faults.

The common problem, in these cases, is to use dynamic invariants for these differences in order to obtain an accurate characterization, such as the application of the Lyapunov exponent, the correlation dimension and the Kolmogorov entropy, etc. The Lyapunov exponents evaluate the sensitivity of a system to changes in initial conditions; a positive Lyapunov exponent physically means that nearby orbits diverge. The existence of positive Lyapunov exponents also implies chaotic dynamics. As a criterion for chaos, one has only to examine the largest Lyapunov exponent and check if it is positive. From the Lyapunov exponents, Lyapunov dimension can be obtained. Kolmogorov entropy, which characterizes the mean velocity of losing information about the system, is also a good criterion for chaos: it is equal to zero for regular motion, infinite for noise, positive and constant for chaotic motion. The measures of dimension evaluate the extent to which orbits will fill a certain subspace and a non-integer dimension is a hallmark of a strange attractor. Many definitions of dimension exist. Here the correlation dimension is introduced. The correlation dimension of a non-linear dynamical system is of value to engineers because it provides an estimation of the number of degrees of freedom that an engineering system possesses.

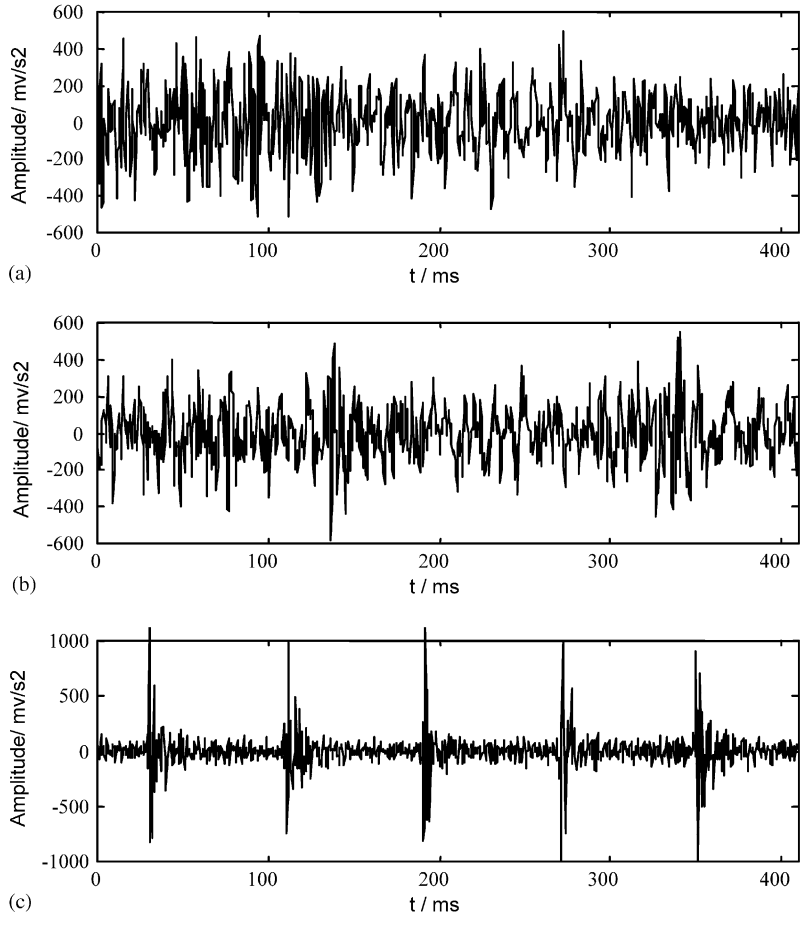

Figure 10. Gearbox vibration signals of different operating conditions: (a) normal, (b) with cracked tooth and (c) with broken tooth.

The Grassberger–Procaccia algorithm of the correlation dimension and its modified formulation, together with the discussions on the influence of data length and noise level on computational accuracy of correlation dimension have been discussed in our previous paper [12]. After the reconstruction of state space, the correlation integral $C_m(r)$ is then defined in the m-dimensional reconstructed space as the probability of finding a pair of vectors whose distance is not larger than r:

$$C_m(r) = \frac{2}{N_m(N_m - 1)} \sum_{i-j>w}^{N_m} \mathrm{H}(r - r_{i,j}), \tag{5}$$

where $\mathrm{H}(x)$ is the Heaviside Step function [$\mathrm{H}(x) = 1$ for $x > 0$ and $\mathrm{H}(x) = 0$ for $x \leqslant 0$] and r is the distance parameter, w is a cut-off parameter which is used to avoid dynamic correlation, $r_{i,j}$ is the distance between two reconstructed vectors. The maximal norm is used because it can save computation time:

$$r_{ij} = \| Y_i - Y_j \| = \max\{|x_{i+l\tau} - x_{j+l\tau}| : 0 \leqslant l \leqslant m - 1\}. \tag{6}$$

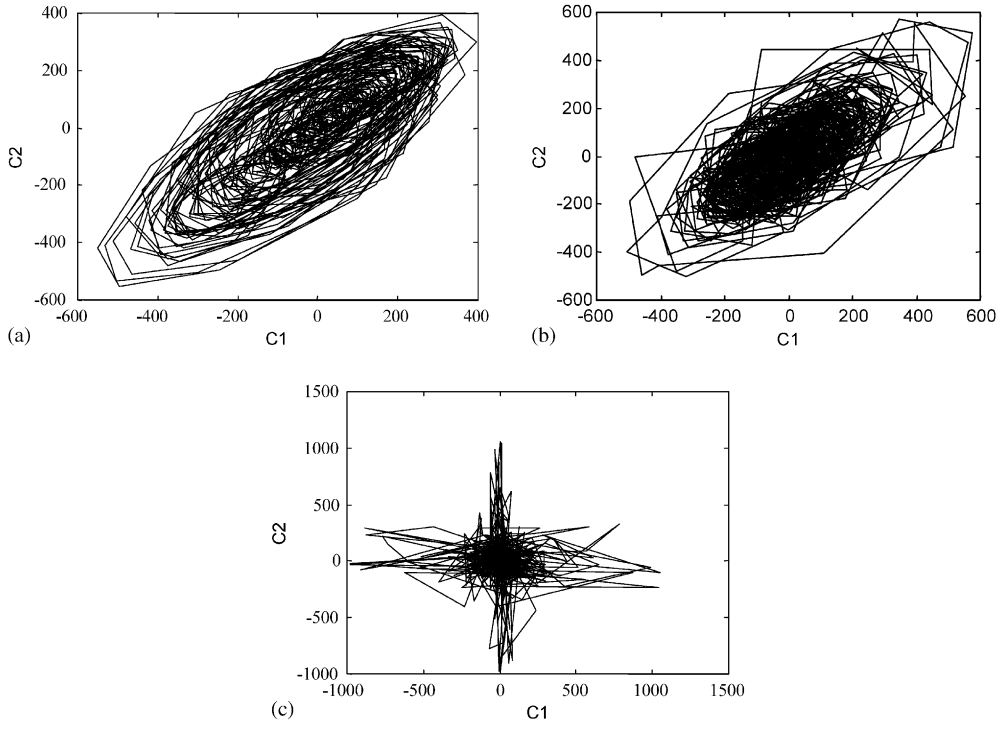

Figure 11. Pseudo-phase portraits of gearbox vibration signals corresponding to different running conditions: (a) normal, (b) with cracked tooth and (c) with broken tooth.

The correlation dimension D_2 is defined as follows:

$$D_2(m) = \lim_{r \to 0} \frac{\ln C_m(r)}{\ln r}. \tag{7}$$

Figure 12 shows the analysis results of correlation dimension of vibration signals in gear systems measured under different operating conditions as shown in Figure 8. The results demonstrate that the state spaces of gear system under different operating conditions constitutes different dimensional attractors due to different kinematic mechanisms. In the case of normal operating condition, the state-space dimension of the attractor is close to 7, which is higher than that obtained under cracked tooth operating condition.

Figure 13 shows the correlation dimension results of the gearbox vibration signals shown in Figure 10. In the case of normal running condition, the correlation dimension is larger than those of the other two abnormal conditions. During the fatigue crack testing process, the correlation dimension decreases as the gear fatigue crack develops. When one of the meshing teeth is finally broken, the dimension reaches a minimum.

4. CONCLUSIONS

In this paper, phase space reconstruction method based on singular value decomposition technique has been introduced. The singular value decomposition is used to determine accurately the embedding dimension. The lag time can then be calculated according to the known relationship among the embedding window length, the lag time and the embedding

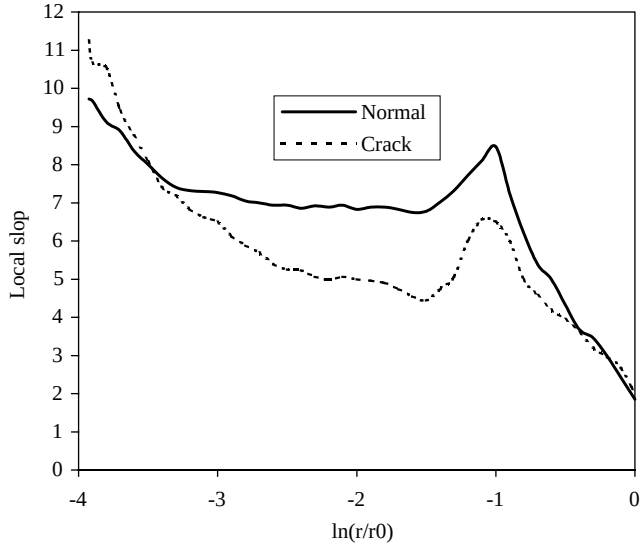

Figure 12. The analysis results of correlation dimension in a gear system vibration signals with different operating conditions shown in Figure 8. The values of embedding dimension and lag time are $(m, \tau) = (16.5)$: ——, normal $D_2 = 7{\cdot}16$; - - -, cracked $D_2 = 4{\cdot}92$.

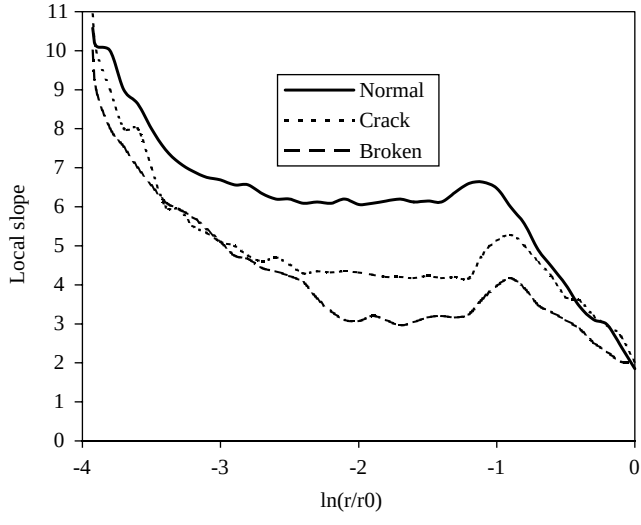

Figure 13. The analysis results of correlation dimension in gearbox vibration signals with different operating conditions shown in Figure 10. The values of embedding dimension and lag time are $(m, \tau) = (14, 5)$. —, normal $D_2 = 6{\cdot}32$; - - -, cracked $D_2 = 4{\cdot}28$; – – –, broken $D_2 = 3{\cdot}23$.

dimension. The singular spectrum has also been found to have the ability to discriminate signal components from those of the contaminated in measured vibration signals.

Pseudo-phase portrait is used to extract qualitative features of machine faults. In general, when one compares the pseudo-phase portraits pertaining to different conditions of a large rotating machine, it is often possible to identify some major differences due to the different dynamic and kinematic mechanisms involved. Although the pseudo-phase

portraits appear as a very complicated solid with an undefined shape for the industrial gear systems, when one carefully compares the pseudo-phase portraits pertaining to different conditions of a gear system, it is also possible to detect some obvious differences due to their different dynamic and kinematic mechanisms. In cases of gear systems condition monitoring, this paper introduces the correlation dimension to quantify these differences in order to obtain a more accurate characterization. From the analysis results presented in this paper, one can see that the pseudo-phase portrait is conceptually simple, and is sensitive to some of the common fault types encountered in engineering. The change of the shape and the position of the pseudo-phase portrait are important factors which can be used to effectively diagnose fault sources and types. Therefore, it is quite possible to apply this proposed pseudo-phase portrait technique to realize the real-time, online computer-aided diagnosis of machine faults.

From the above analysis, one can conclude that diagnostic modules based on non-linear dynamics can add useful diagnostic information for rotating machinery in particular and mechanical systems in general, supplementing the traditional methods. Further work in this diversion should seek to collect as much as possible the actual industrial data. Moreover, it will be necessary to establish the correlation between diagnostic parameters and damage parameters for the final diagnostic system.

REFERENCES

1. C. L. Chen and H. T. Yao 1988 *Non-linear Dynamics* **16**, 71–90. Chaos in the imbalance response of a flexible rotor supported by oil film bearings with non-linear suspension.
2. P. Goldman and A. Muszynska 1994 *Journal of Vibration and Acoustics* **116**, 541–547. Dynamic effects in mechanical structures with gaps and impacting: order and chaos.
3. Muszynska and P. Goldman 1995 *Chaos, Solitons & Fractals* **5**, 1683–1704. Chaotic responses of unbalanced rotor/bearing/stator systems with looseness or rubs.
4. F. L. Chu and Z. S. Zhang 1997 *International Journal of Engineering Science* **35**, 963–973. Periodic, quasi-periodic and chaotic vibrations of a rub-impact system supported on oil film bearings.
5. P. C. Muller, J. Bajkowski and D. Soffker 1994 *Non-linear Dynamics* **5**, 233–254. Chaotic motions and fault detection in a cracked rotor.
6. R. J. Comparin and R. Singh 1990 *Journal of Mechanical Design* **112**, 237–245. An analytical study of automotive neutral gear rattle.
7. M. L. Adams and I. A. Abu-mahfouz 1994 *Proceedings of IFTOMM Fourth International Conference on Rotor Dynamics. Chicago, U.S.A.* September, 29–39. Exploratory research on chaos concepts as diagnostic tools for assessing rotating machinery vibration signatures.
8. W. J. Wang, J. Chen, X. K. Wu and Z. T. Wu 2001 *Mechanical Systems and Signal Processing* **15**, 679–705. The application of some non-linear methods in rotating machinery fault diagnosis.
9. D. Logan and J. Mathew 1996 *Mechanical Systems and Signal Processing* **10**, 251–264. Using the correlation dimension for vibration fault diagnosis of rolling element bearing—2. Selection of experimental parameters.
10. J. D. Jiang, J. Chen and L. S. Qu 1999 *Journal of Sound and Vibration* **23**, 529–542. The application of correlation dimension in gearbox condition monitoring.
11. C. Craig, R. D. Neilson and J. Penman 2000 *Journal of Sound and Vibration* **231**, 1–17. The use of correlation dimension in condition monitoring of systems with clearance.
12. W. J. Wang, J. Chen and Z. T. Wu 2000 *ImechE, Journal of Mechanical Engineering Science* **C214**, 921–930. The application of correlation dimension in large rotating machinery fault diagnosis.
13. F. Takens 1981 in *Lecture Notes in Mathematics* (D. A. Rand and L. S. Young, editors), 366–342. Berlin: Springer. Detecting strange attractors in turbulence.
14. M. Albona, J. Muench and C. Schwartz 1988 *Physical Review A*. **38**, 3107–3126. Singular-value decomposition and the Grassbergar–Procaccia algorithm.
15. M. Fraser and H. L. Swinney 1986 *Physical Review A* **33**, 1134–1140. Independent coordinates for strange attractors from mutual information.

16. T. Buzug and G. Pfister 1992 *Physica D* **58**, 127–140. Comparison of algorithms calculating optimal parameters for delay time coordinates.
17. W. Libert, K. Pawelzik and H. G. Schuster 1991 *Europhysics Letters* **14**, 521–527. Optimal embeddings of chaotic attractors from topological considerations.
18. M. Albano, A. Passmante and M. E. Farrell 1991 *Physica D* **54**, 85–97. Using higher-order correlations to define an embedding window.
19. J. C. Roux, R.H. Simoy and H. L. Swinney 1983 *Physica D* **8**, 257–266. Observation of a strange attractor.
20. Y. I. Neymark 1972 Pattern Recognition and Medical Diagnostics. Moscow: Nauka (in Russian).
21. P. S. Landa and M. G. Rosenblum 1991 *Physica D* **48**, 232–254. Time series analysis for system identification and diagnostics.
22. S. Broomhead and G. P. King 1986 *Physics D* **20**, 217–236. Extracting qualitative dynamics from experimental data.
23. D. Kugiumtzis 1996 *Physica D* **95**, 13–28. State space reconstruction parameters in the analysis of chaotic time series-the role of the time window length.
24. C. Cempel 1999 *Conference Proceedings of Damage Assessment of Structure, DAMAS' 99, Dublin*, June'99, 172–188. Innovative developments in systems condition monitoring.
25. J. C. Schouten, F. Takens and C. M. Van den Bleek 1994 *Physical Review E*. **53**, 1851–1891. Estimation of dimension of a noisy attractor.
26. E. N. Lorenz 1963 *Journal of Atmospheric Science* **26**, 130–136. Deterministic nonperiodic flow.
27. R. B. Randall 1982 *Journal of Mechanical Design* **104**, 259–267. A new method of modelling gear faults.
28. P. D. McFadden 1986 *American Society of Mechanical Engineers Journal of Vibration, Acoustics, Stress, and Reliability in Design* **108**, 165–170. Detecting fatigue cracks in gear by amplitude and phase demodulation of the meshing vibration.
29. Capdessus, M. Sidahmed and J. L. Lacoume 2000 *Mechanical Systems and Signal Processing*, **14**, 371–385. Cyclostationary processes: application in gear faults early diagnosis.
30. W. J. Staszewski, K. Worden and G. R. Tomlinson 1997 *Mechanical Systems and Signal Processing* **11**, 673–692. Time–frequency analysis in gearbox fault detection using the Wigner–Ville distribution and pattern recognition.
31. P. D. McFadden 1994 *Proceedings of an International Conference on Condition Monitoring, Swansea, U.K.*, 172–183. Application of the wavelet transform to early detection of gear failure by vibration analysis.

APPENDIXA: NOMENCLATURE

A	trajectory matrix
B	covariance matrix
$C_m(r)$	correlation integral
D_2	correlation dimension
$\mathrm{H}(x)$	Heaviside step function
m	embedding dimension
N	length of the original time series
$N_L^{-1/2}$	normalization coefficient
N_m	length of the reconstructed state-space vector
x_i	original time series
y_i	reconstructed state-space vector
σ_j	normalized singular value
τ	lag time
τ_w	embedding window length